Precision mass measurements of rare isotopes near $N = Z = 33$ produced by fast beam fragmentation

P. Schury,[1,2,*] C. Bachelet,[1] M. Block,[1] G. Bollen,[1,2] D. A. Davies,[1,3] M. Facina,[1] C. M. Folden III,[1] C. Guénaut,[1] J. Huikari,[1] E. Kwan,[1,2] A. Kwiatkowski,[1,2] D. J. Morrissey,[1,3] R. Ringle,[1,2] G. K. Pang,[1,3] A. Prinke,[1,2] J. Savory,[1,2] H. Schatz,[1,2] S. Schwarz,[1] C. S. Sumithrarachchi,[1,3] and T. Sun[1,2]

[1]*National Superconducting Cyclotron Laboratory, East Lansing, Michigan 48824, USA*

[2]*Department of Physics and Astronomy, Michigan State University, East Lansing, Michigan 48824, USA*

[3]*Department of Chemistry, Michigan State University, East Lansing, Michigan 48824, USA*

(Received 24 January 2007; published 2 May 2007)

Mass measurements of ^{63,64}Ga, ^{64,65,66}Ge, ^{66,67,68}As and ^{69}Se performed at the LEBIT facility at the NSCL by Penning trap mass spectrometry are presented. The rare isotopes were produced by fast beam fragmentation and in-flight separation, then converted to a low energy beam using a gas stopping technique. Masses of the $N = Z$ nuclei ^{66}As and ^{64}Ge have been determined with uncertainties of $\delta m/m = 5 \times 10^{-7}$ and 6×10^{-8}, respectively, representing a more than ten-fold improvement in precision over previous measurements. For ^{63,64}Ga, ^{65,66}Ge, ^{67,68}As, and ^{69}Se relative mass uncertainties of $\delta m/m < 5 \times 10^{-8}$ were obtained. ^{69}Se is found to be 135 keV more bound than the value listed in the 2003 Atomic Mass Evaluation. Using theoretical Coulomb shift energies in combination with the experimental mass values for ^{65,66}Ge, ^{67}As, and ^{69}Se, masses for ^{65}As, ^{66,67}Se, and ^{69}Br are predicted with an estimated uncertainty of 100 keV. These mass values, in conjunction with our measurements, were used to calculate improved effective lifetimes of the rp-process waiting point nuclei ^{64}Ge and ^{68}Se. We find that ^{64}Ge is less of a waiting point while ^{68}Se poses a larger delay in the rp-process than previously thought. The improved mass values in this region were also used to investigate the neutron-proton pairing energy of odd-odd $N = Z$ nuclei.

DOI: 10.1103/PhysRevC.75.055801 PACS number(s): 21.10.Dr, 26.30.+k, 07.75.+h, 27.50.+e

I. INTRODUCTION

The rapid proton capture process (rp-process) is believed to drive type I X-ray bursts in accreting neutron stars, producing elements beyond iron [1,2]. The rp-process proceeds along isotonic chains until proton capture is inhibited, either by proton decay or photodisintegration. When the rp-process reaches an equilibrium between proton capture and loss, the process must wait for the β-decay of the equilibrium nucleus before it can continue [1]. These nuclei are the so-called waiting point nuclei.

The lifetimes of waiting point nuclei are of particular interest as they set the time scale for the rp-process, which shapes the observed X-ray burst light curves [3–5]. The waiting point lifetimes also determine the final composition of the burst ashes, important for reliable predictions of the composition of neutron star crusts [6]. The effective lifetimes of waiting point nuclei strongly depend on proton separation energies which can be directly determined from mass differences. The effective lifetime of a nucleus in an X-ray burst is exponentially dependent on its proton separation energy, Q_p. As a consequence, accurate X-ray burst model calculations require mass values with small uncertainties, desirably less than 10 keV [5,6]. Using such precise mass values, X-ray burst model calculations can be compared with observed X-ray burst light curves to improve our understanding of the composition of neutron star crusts.

However, as the $N = Z$ line approaches the proton drip line, and therefore the rp-process pathway, near $N = Z = 33$ [5], mass uncertainties in excess of 100 keV are typical at present. This region of the nuclear chart is where the rp-process is believed to encounter three long-lived waiting point nuclei: ^{64}Ge, ^{68}Se, and ^{72}Kr [6]. Reduced mass uncertainties at and near these waiting points will improve our understanding of the rp-process timescale.

Mass measurements in this region are not only of interest for astrophysics. It is experimentally known that the neutron-proton pairing energy is considerably increased for $N = Z$ nuclei as compared to nearby nuclei with $N \neq Z$. This increased pairing energy, first introduced by Wigner [7], has been interpreted as $T = 0$ pairing [8] and has been explained in the *sd*-shell as a direct effect of SU(4) symmetry [9]. Experimental values from which neutron-proton pairing energies of $N = Z$ nuclei can be calculated cease to exist in this region, but there is speculation that the Wigner energy may vanish as the $N = Z$ line approaches ^{100}Sn due to SU(4) symmetry breaking from large Coulomb and spin-orbit interactions [10]. However, it has also been speculated that there may be a midshell restoration of the Wigner energy due to pseudo-SU(4) symmetry in the *pf*-shell [9]. New mass measurements along with improvements in masses of heavier $N = Z$ nuclei can help to answer this open question.

The study of the short-lived Ge, As, and Se isotopes in the region near $N = Z = 33$ has been largely limited to facilities utilizing fast beam fragmentation or fusion-evaporation reactions. Mass measurements for these isotopes have until recently been limited to time-of-flight measurements,

*Corresponding author. Email address: schury@nscl.msu.edu

supplemented by β-decay studies. For example, the only previous direct mass measurement for ^{66}As was performed in a time-of-flight experiment with SPEG at GANIL, where an uncertainty of 680 keV was obtained [11].

In recent years a number of facilities with Penning trap mass spectrometers have made advances into this region. At ISOLDE/CERN, mass measurements of ^{63,64}Ga [12] were preformed with ISOLTRAP, making use of advances in selective laser ionization. Furthermore, using the IGISOL technique with fusion-evaporation reactions, JYFLTRAP has recently measured the mass of ^{62}Ga [13]. The Canadian Penning Trap (CPT) at Argonne National Laboratory has recently performed mass measurements of ^{64}Ga, ^{68}As and of the waiting point nuclei ^{68}Se and ^{64}Ge, provided via fusion-evaporation reactions [14,15].

The Coupled Cyclotron Facility at the NSCL provides beams of short-lived isotopes produced by heavy-ion fragmentation and in-flight separation [16]. At the Low Energy Beam and Ion Trap (LEBIT) facility at the NSCL, we have recently succeeded in performing the first Penning trap mass measurements on isotopes produced via projectile fragmentation and in-flight separation of ^{37,38}Ca [17,18]. Here we report high-precision mass measurements of isotopes in the $N = Z = 33$ region performed at the LEBIT facility.

II. APPARATUS

Figure 1 gives a schematic overview of the LEBIT facility and its main components. The gas stopping station [19,20] is used to thermalize intermediate energy (80–120 MeV/nucleon) rare isotopes and convert them into a low energy beam. The beam cooler-and-buncher system [21] converts the ion beam into short pulses which are then captured in a high precision Penning trap mass spectrometer [22].

A. Gas stopping station

Rare isotope ions delivered from the A1900 fragment separator [16] are slowed in a solid degrader system before the beam passes through a beryllium window and enters the gas cell. The degrader system consists of glass plates and a glass wedge. The glass plates are parallel at the level of 1 μm and can be rotated to adjust their effective thickness, providing a degree of control over where inside the gas cell the ions come to rest. The glass wedge is placed at a point in the beam line with a horizontal momentum dispersion to compensate for the momentum spread [23] of the ions coming from the A1900. This reduces the range distribution of the ions in the gas to the limit produced by range straggling and nonuniformities in the degraders.

The gas cell uses a 50 cm long volume filled with ultra-high purity helium gas at a pressure of $\approx$500 mbar. A set of electrodes inside the gas cell provides an electrostatic field to pull the ions close to an extraction nozzle through which the ions are swept out of the gas cell by gas flow.

Extracted ions are carried by the gas jet into an ion guide system. The system is composed of a set of three radio-frequency quadrupole (RFQ) ion guides. These RFQ ion guides, part of a differential pumping system, provide ion transport into high vacuum from the relatively high pressure region immediately following the gas cell. The first RFQ is segmented to allow the superposition of an electrostatic potential gradient to pull the ions through the gas, which in this section can have a pressure as high as 0.05 mbar. The second, miniature, RFQ provides an efficient barrier for differential pumping while transporting ions into the third RFQ. The third ion guide can be used as an RFQ mass filter.

Near the end of this mass filter, a "needle" electrode can be inserted into the path of the ions to collect radioactive ions. After collection, it can be moved in range of a plastic scintillator β-detector for measuring the activity collected. As an alternative, a retractable silicon surface barrier β-detector inserted downstream from the ion guides can be used to monitor the activity.

B. Beam cooler and buncher

After being transported into high vacuum by the ion guide system, ions are accelerated to 5 keV/q and transported to the cooler-buncher system (see Fig. 1). A test ion source capable of delivering alkali or noble gas ions is installed perpendicular to the beam line prior to the beam cooler. Ions from this source can be used for tuning the system as well as for providing ions for reference mass determinations.

The cooler-buncher system [21] converts the continuous beam delivered from the gas cell into ion pulses suitable for capture by the Penning trap [24]. It consists of a precooler section and an ion trap section. The precooler is a gas filled RFQ ion guide operated with neon or helium gas at $\approx 2 \times 10^{-2}$ mbar. The incoming ion beam is slowed down, cooled and guided into the trap section by a miniature ion

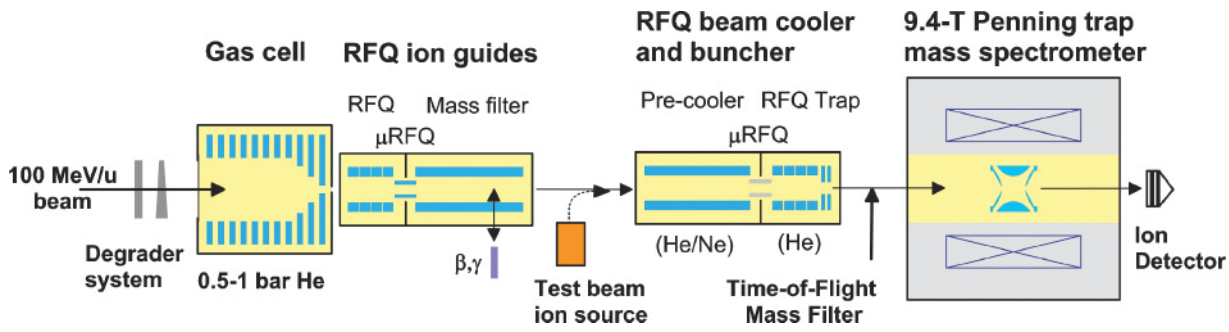

FIG. 1. (Color online) Schematic overview of the LEBIT facility at the NSCL.

guide. In addition to beam cooling, the precooler allows for collision induced dissociation (CID) of molecular contaminants if needed. Ions are finally accumulated in the trap section. The trap section is a gas filled linear RFQ trap operated in an environment of $\approx 8 \times 10^{-4}$ mbar high-purity (99.999%) helium. The axial trapping potential is formed by a series of annular electrodes encircling the RF electrodes. To reduce charge exchange during storage as well as improve beam cooling, the cooler-and-buncher electrodes are cryogenically maintained at temperatures below 0°C.

After cooling for typically 20–30 ms, the annular electrode voltages are switched to create an accelerating field for fast ion ejection. Fast MOSFET switches are used for this purpose, allowing for switching times of about 100 ns. This fast switching, along with an appropriate electric field shape, creates ion pulses of submicrosecond duration.

After ejection from the buncher, the ions travel ≈2.5 m to a fast deflector which acts as a time-of-flight mass separator. Ions of a desired mass number can be selected and any molecular break-up products from CID in the cooler can be rejected. At the same location, a microchannel plate (MCP) ion detector can be inserted for time-of-flight mass identification of the ions ejected from the buncher. This mass identification is useful for optimization of CID in the cooler.

C. Penning trap

The ions are electrostatically transported to the LEBIT Penning trap mass spectrometer, then injected into the trap through a "Lorentz" steerer [25] inside the magnetic field. This device allows the ions to be injected into the Penning trap off axis, imparting an initial magnetron orbit needed for the cyclotron frequency determination scheme used by the LEBIT Penning trap mass spectrometer.

The high-precision hyperbolic electrode system of the Penning trap is mounted in a vacuum chamber inside the bore of a 9.4 T persistent superconducting solenoidal magnet, with the trap positioned in the central homogeneous region of the magnetic field. The trap, constructed to introduce minimal electric and magnetic field imperfections, features an eight-fold segmented ring electrode for RF-excitation of the ion motion. A high magnetic field stability is achieved by regulation of the liquid helium cryostat pressure, and an active compensation for the natural field decay is used.

The LEBIT Penning trap mass spectrometer makes use of the time-of-flight resonance detection method [26], detailed below, for determination of the ion cyclotron frequency. In order to measure an ejected ion's time-of-flight, a series of drift tube electrodes electrostatically transport ions from the Penning trap to an MCP ion detector in a Daly configuration [27]. As an alternative to the Daly detector, a silicon surface-barrier β-detector can be used for the detection of the radioactive decay of ions ejected from the trap.

III. PROCEDURE

Each ion stopped in the gas cell creates, typically, $10^6 - 10^7 e^-$-He^+ pairs. The high ionization density in the gas cell and the high ionization potential of helium gives a high probability for charge exchange with residual gas molecules, such that even sub-ppb impurities in the gas result in molecular ion beams several orders of magnitude greater than the rare isotope beam extracted from the gas cell.

Due to these high rates of contaminant ions extracted from the gas cell on top of the rare isotope ions of interest, careful ion preparation is an important aspect of the measurements reported here. In addition to being cold, i.e. occupying only a small phase space, the ion ensemble reaching the Penning trap should contain only one ion species to avoid ion-ion interactions which would lead to shifts in the cyclotron frequencies. This requires appropriate operation of the gas cell system to maximize stopping and extraction efficiencies of the desired rare isotope species, identification of molecules formed by the rare isotopes, purification of the desired beam and identification and in-trap removal of any contaminants remaining after purification.

A. Radio-molecular identification

The A1900 fragment separator generally provides isotonic "cocktail" beams. Three such cocktail beams were used for these measurements: (^{66}As, ^{65}Ge, ^{64}Ga), (^{67}As, ^{66}Ge, ^{65}Ga), and (^{69}Se, ^{68}As, ^{67}Ge). Based upon the Z-dependence of the stopping power, the degrader thickness was adjusted to provide optimized stopping for each isotope [20], verified through stopping range measurements [20] and subsequent activity measurements of the extracted beam.

In previous experiments it was found that ^{38}Ca formed water adduct molecular sidebands of $[^{38}Ca(H_2O)_n]^{2+}$ with $n = \{1, 2, 3, 4\}$ [17]. Therefore, after optimizing beam stopping and extraction from the gas cell, we determined the molecular form of the desired isotope using the mass filter and one of the β-detectors. Figure 2 shows the results of mass-versus-activity scans for ^{65}Ge and ^{67}As. The results indicate that arsenic was delivered as $AsHe^+$ and germanium as GeH^+. In similar measurements, Se and Ga were found to be delivered from the gas cell as Se^+ and Ga^+.

B. Beam purification

Preparation of the beam extracted from the gas cell makes use of a multi-stage beam purification system. The first stage in the beam purification is the RFQ mass filter after the gas

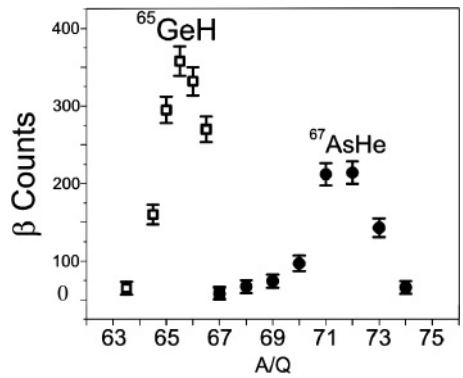

FIG. 2. Counts recorded on β-detector as a function of mass filter setting, together with molecular assignment.

cell, which selectively transports ions of a desired mass-to-charge ratio with a resolving power tunable to R > 100. After this stage the beam consists primarily of ions of the chosen mass-to-charge ratio, although some molecular ions may still have rates which are orders of magnitude greater than that of the desired rare isotope ions.

The second stage is collision-induced dissociation (CID) of molecular contaminants and/or rare isotope molecular ions, using the beam cooler-and-buncher as a gas target. When the molecular ions are injected into the cooler, collision with the buffer gas can cause molecular excitation. If the molecular excitation energy is greater than the energy of a molecular bond, a neutral molecule can be "evaporated" from the system. This process typically results in the the removal of CH_4, CO, or H_2O from hydrocarbon molecular ions and the removal of adducts such as He or H_2O from the rare isotope ions. For a more thorough review of collision-induced dissociation, see [28].

The third stage in the beam purification is the use of the pulsed beam steerer, mentioned earlier, as a time-of-flight mass filter. This step allows the exploitation of the fact that after CID the rare isotope ions are no longer mixed with an ensemble of isobaric contaminants. By optimizing the beam cooler-and-buncher ejection optics to create a time focus at the time-of-flight mass filter, a mass resolving power of >100 can be achieved.

With the Penning trap operated in a direct transmission mode, the molecular state of the rare isotopes after ejection from the beam cooler-and-buncher can be determined by measuring activity at the β-detector following the Penning trap as a function of the time-of-flight mass filter setting. From activity scans with this scheme, it was found that the helium adduct was removed from $^{67}AsHe^+$, but $^{65}GeH^+$ remained intact.

The final step in the beam purification process is the determination of any yet remaining isobaric contaminants. The high resolving power of the LEBIT Penning trap system allows for unambiguous determination of contaminants. Once these contaminants are identified, it is possible to selectively remove them from the trap prior to the mass measurement procedure.

After being captured in the trap, ion are initially exposed to an azimuthal dipole RF-field for, typically, 10–20 ms. This dipolar RF-field is generated by the superposition of the signals from up to six frequency generators, each operated at the reduced cyclotron frequency of a known (or suspected) contaminant. This selectively removes those contaminant ions from the trap by increasing the amplitudes of the their cyclotron motion [29].

C. Determination of the ion cyclotron frequency

Ions ejected from the buncher are captured in the Penning trap on a magnetron orbit. After in-trap removal of contaminants, a quadrupolar RF-field with a frequency close to the expected cyclotron frequency of the ion of interest is applied for a duration T_{RF} with an amplitude V_{RF} such that initial magnetron motion is fully converted into reduced cyclotron motion [26]. This conversion is accompanied by a large increase in radial energy. The ions are then ejected from the trap and their time of flight to the MCP ion detector is recorded.

When the ion passes through the inhomogeneous magnetic field, on the way to the MCP, radial energy is converted into axial energy. Thus, a resonantly excited ion with increased radial energy will have a shorter time of flight than a nonexcited ion. The process is then repeated again with a newly captured ensemble of ions for a different excitation frequency, ν_{RF}. In this way, we measure the mean time of flight of the ion ensemble as a function of the excitation frequency. The frequency of minimum time-of-flight is the cyclotron frequency of the ion,

$$\nu_c = \frac{q}{2\pi m} \cdot B \tag{1}$$

from which the ion mass can be deduced.

For the measurements discussed herein, excitation times in the range of T_{RF} = 200 ms to 500 ms were generally used. As an exception, due to its short half-life ($T_{1/2}$ = 96 ms), an excitation time of 50 ms was used for ^{66}As. In order to minimize systematic effects from ion-ion interactions, the number of ions in the trap was kept low, in nearly all cases less than five detected ions per trapping cycle. Table I lists the isotopes studied in five different beam times together with the reference ion and the mean number of ions detected per cycle for all measurements reported in this paper.

Figure 3 shows typical cyclotron resonance curves obtained for ^{67}As and ^{64}GeH. From the fit of the theoretical curve [30], the center frequency is obtained, which corresponds to the cyclotron frequency, ν_c, of the ion. A total of 62 resonance curves were obtained for rare isotopes in the course of this work.

In order to determine the mass, the magnitude of the magnetic field must be determined. This is done by obtaining cyclotron resonance curves for an ion species with well-known mass before and after obtaining each cyclotron resonance curve for the species of interest and interpolating the value of the magnetic field during the measurement of the species

TABLE I. Isotopes studied, references used, mean number of ions detected per cycle and total number of resonance curves measured during five online experiments. All ions were singly charged.

Experiment Run No.	Species	Reference	$\overline{\text{ions}}$/cycle	Number of measurements
1	^{67}As	^{86}Kr	1.2	5
2	^{67}As	^{86}Kr	0.6	1
3	^{67}As	^{85}Rb	0.5	15
2	^{65}GeH	C_5H_5	2.3	14
3	^{65}GeH	^{85}Rb	0.6	3
4	^{65}GeH	C_5H_2	0.6	1
3	^{66}As	^{85}Rb	0.002	4
5	^{66}GeH	C_5H_5	0.8	4
5	^{68}As	CF_3	0.2	3
5	^{69}Se	CF_3	0.6	5
5	^{64}GeH	HSO_2	0.5	3
5	^{64}Ga	C_5H_2	2.4	3
5	^{63}Ga	C_5H_2	2.0	1

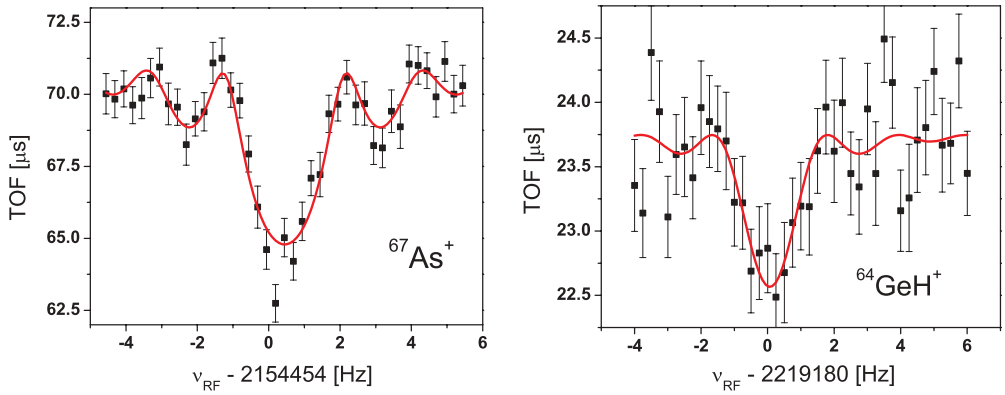

FIG. 3. (Color online) Left: Time of flight versus excitation frequency for $^{67}As^+$ ions ejected from the Penning trap after a 500 ms quadrupolar excitation. The solid line is a fit of the theoretical line shape [30] to the data. Right: Similarly for $^{64}GeH^+$ ions.

of interest. In the measurements reported herein, a number of different reference ions were used. Krypton and rubidium isotopes were obtained from the test ion source, while the hydrocarbon molecular ions and HSO_2^+ were obtained from the gas cell.

IV. DATA EVALUATION

The primary data from Penning trap mass measurements are the cyclotron frequency ratios, $R = \nu_c/\nu_{c,ref}$, where ν_c is the cyclotron frequency of the species of interest and $\nu_{c,ref}$ is the cyclotron frequency of the reference species. For each measurement, the cyclotron frequency is determined by fitting the analytical time-of-flight cyclotron resonance line shape [30] to the data. The mass of the species of interest is extracted from the cyclotron frequency ratio using $M = R\cdot(M_{ref} - m_e) + m_e$, where m_e is the mass of an electron. The values for m_e and M_{ref} are taken from the 2003 Atomic Mass Evaluation (AME'03) [31]. In principle, the difference in ionization potentials of the reference and species of interest should be taken into account, but within the uncertainties of the measurements presented herein it is negligible.

In order to account for decay of the magnetic field between measurements, each measurement of the species of interest was bracketed by two reference measurements. The reference frequency used for the frequency ratio, $\nu_{c,ref}$, is interpolated from the references taken before, $\nu_{c,ref1}$, and after, $\nu_{c,ref2}$, the measurement of the species of interest. The reference frequency is calculated with a linear interpolation as

$$\nu_{c,ref} = \nu_{c,ref1} - (\nu_{c,ref1} - \nu_{c,ref2}) * \frac{t_m - t_1}{t_1 - t_2}, \qquad (2)$$

where t_1, t_2, and t_m are the mean time of the anterior reference, posterior reference and measurement, respectively. The mean time refers to the time halfway between the start and end of a measurement. The statistical uncertainty associated with the frequency ratio is given by standard propagation of errors techniques.

Sources of systematic error include nonlinear decay of the magnetic field, cyclotron frequency shifts from ion-ion interactions [32] and mass dependent effects due to trap imperfections [33]. It has been demonstrated [17] that the nonlinear decay of the magnetic field of the LEBIT spectrometer is negligible on the 10 ppb level when reference measurements are performed at intervals of less than 2 h. Thus any effects from a nonlinear term in the decay were ignored, since reference measurements were taken on intervals of, typically, 30–60 min except in the case of ^{66}As, where the typical intervals were 3–4 h. A statistical uncertainty of $\delta m/m \approx 10^{-7}$ was achieved, compared to which any systematic uncertainty from nonlinear field decay is negligible.

To probe possible mass dependent systematic effects, during one of the runs a set of three mass measurements of $^{39}K^+$ was made using $^{85}Rb^+$ as a reference. The results from these data indicate a mass dependent systematic error term of $\delta m/m = 5(5) \times 10^{-10}/\Delta u$, where Δu is the mass difference between measured and reference ions in atomic mass units. For use in the data analysis, we have adopted a value of $\delta m/m = 5 \times 10^{-10}/\Delta u$ as the maximum mass dependent systematic uncertainty.

Frequency shifts that may be caused by ion-ion interactions were investigated by performing a count rate analysis. For each data set with a sufficient distribution of count rates, including reference measurements, the data were sorted into bins by number of detected ions. Cyclotron frequencies were determined for each counting bin. Using a linear fit to these data, and taking the detector efficiency into account, the cyclotron frequency of a single trapped ion was determined. In instances where there were insufficient data to properly fit the binned data, this analysis could not be performed. Such was the case for all measurements of ^{66}As and ^{68}As as well as all measurements from the second run with ^{67}As and most measurements of ^{69}Se.

While there is no clear evidence that our measurements suffer any frequency shifts due to ion-ion interactions, we chose to be conservative and, where available, use the count-rate adjusted data, which have a somewhat larger statistical uncertainty to account for any ion-ion interactions. Table II lists the mean frequency ratio for each set of measurements, with the statistical uncertainty listed in parenthesis.

In the cases of $^{66,68}As$, the Birge ratios [34] were found to be 1.7(2) and 1.8(3), respectively, indicating that the uncertainties of the individual measurements were underestimated. In all other cases the data sets had Birge ratios of $\lesssim 1$. To be

TABLE II. Mean frequency ratios obtained for each set of measurements. Values were derived from count-rate analyzed data wherever possible. Listed uncertainties are statistical. In the case of ^{66,68}As the listed uncertainty has been increased to account for a large Birge ratio, see the text.

Nuclide	Reference	Frequency ratio
^{63}Ga	$^{12}C_5H_2$	1.01489389(11)
^{64}Ga	$^{12}C_5H_2$	1.030979398(44)
^{64}GeH	$H^{32}S^{16}O_2$	0.99688922(62)
^{65}GeH	$^{12}C_5H_5$	1.013961997(66)
^{65}GeH	$^{12}C_5H_2$	1.063396513(69)
^{65}GeH	^{85}Rb	0.776653759(73)
^{66}GeH	$^{12}C_5H_5$	1.029252824(40)
^{66}As	^{85}Rb	0.77661811(38)
^{67}As	^{86}Kr	0.779171859(34)
^{67}As	^{86}Kr	0.77917095(35)
^{67}As	^{85}Rb	0.788337366(20)
^{68}As	$^{12}C^{19}F_3$	0.984659141(81)
^{69}Se	$^{12}C^{19}F_3$	0.999191318(23)

conservative, in the case ^{66,68}As we use the outer error instead of the inner error, i.e., increase the uncertainties listed in Table II by a factor equal to the Birge ratio.

V. RESULTS AND DISCUSSION

A. Atomic masses

The mass excesses determined in the present work for ^{63,64}Ga, ^{64,65,66}Ge, ^{66,67,68}As, and ^{69}Se are given in Table III. These are based on the weighted mean of the mass excesses obtained from the individual frequency ratios given in Table II. An additional error of $\delta m/m = 5 \times 10^{-10}$/u was included in cases with non-isobaric reference ions to account for possible mass dependent effects. The mass value for the reference ions are based on values listed in the 2003 Atomic Mass Evaluation (AME'03) [31]. For the Ge isotopes, which were measured as GeH^+, the mass excess values listed have been obtained by subtracting the hydrogen mass excess from the molecular mass excess, ME(^{A}Ge) = ME(^{A}GeH)−ME(H).

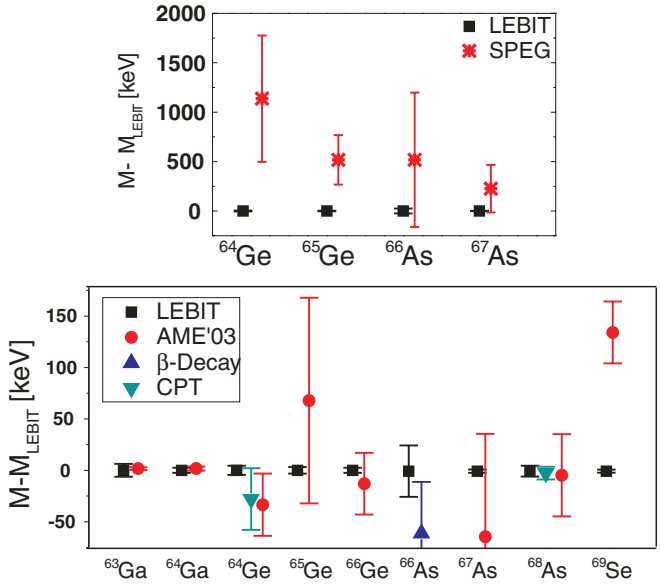

FIG. 4. (Color online) Comparison of measurements presented in this paper with literature values from AME'03 [31], time-of-flight measurements with SPEG [11], Penning trap measurements from CPT [15] and β end-point measurements [36].

The new measurements are within 1-σ deviation of the values listed in AME'03, with the exception of ^{69}Se (-4.5σ) and ^{64}Ge ($+1.1\sigma$). In particular, the new values are in excellent agreement with recent Penning trap measurements from other facilities. For instance, mass measurements of ^{63,64}Ga [12] recently performed at ISOLDE/CERN with ISOLTRAP [37] and already included in AME'03 agree with our values. Also, while our value for the mass of ^{64}Ge has a much higher precision than previous measurements it agrees with recent measurements made with the CPT at Argonne National Lab [15], as does our value for ^{68}As [14].

The isotopes ^{64,65}Ge, and ^{66,67}As have previously been measured via time-of-flight mass spectrometry using SPEG at GANIL [11]. Figure 4 (top) compares our mass excess

TABLE III. Mass excess values obtained in this work. The values from the 2003 Atomic Mass Evaluation and their deviation from values obtained in this work are listed for comparison. The column ME$_{Other}$ lists measurements from other groups which were not included in the 2003 Atomic Mass Evaluation. All values are given in keV.

Species	ME$_{LEBIT}$	ME$_{AME'03}$	ME$_{Other}$	ME$_{LEBIT}$-ME$_{AME'03}$
^{63}Ga	−56545.4(6.3)	−56547.1(1.3)		1.7(6.4)
^{64}Ga	−58832.6(2.5)	−58834.3(2.0)	−58832.5(3.9) [35]	1.7(3.2)
^{64}Ge	−54315.7(3.8)	−54350(30)	−54344(30) [35]	−34(30)
^{65}Ge	−56480.6(1.2)	−56410(100)		71(100)
^{66}Ge	−61607.0(2.4)	−61620(30)		−13(30)
^{66}As	−52018(30)	−51500(680)	−52057(50) [36]	518(681)
^{67}As	−56586.0(1.1)	−56650(100)		−64(100)
^{68}As	−58896.2(5.3)	−58900(40)	−58894.4(3.1) [14]	−4(40)
^{69}Se	−56434.6(1.5)	−56300(30)		135(30)

TABLE IV. Mass excesses for the mirrors of nuclei presented earlier in this work, calculated using Coulomb displacement energies [5], compared with Audi-Wapstra extrapolations from AME'03 [31]. All values are in keV.

Species	$ME_{This\ work}$	$ME_{AME'03}$	Deviation
^{65}As	−46776(100)	−46980(300)	−204(316)
^{66}Se	−41833(100)	−41720(300)	113(316)
^{67}Se	−46548(100)	−46490(200)	58(224)
^{69}Br	−46264(100)	−46480(110)	−216(149)

values for these four isotopes with values from SPEG. Figure 4 (bottom) compares the mass excess values presented in this work with values from the literature. The data are divided into two graphs to simplify comparisons, as the scale of uncertainties, and the deviations from our measured values, for the four data points from SPEG [11] are larger in comparison to the rest of the data.

As can be seen from Fig. 4, the SPEG values overlap the present values for the heavier isotopes, but not for the lighter ones. From Fig. 4 it appears that the SPEG masses may suffer from a systematic bias. This may be related to their use of ^{69}Se as a reference mass. The mass of ^{69}Se was previously determined in two ^{69}Se(εp)^{68}Ge decay studies [38,39]. While they are consistent with each other, they differ from our mass excess values by more than 4σ. We also note that the ^{66}As β-decay study of Davids *et al.* [36], which has been disregarded in previous editions of the Atomic Mass Evaluation due to discrepancies with expected S_{2n} values, agrees with the Q_β value derived from the present measurements.

B. Mass predictions from Coulomb displacement energies

New predictions for the masses of the nuclei ^{65}As, ^{66,67}Se and ^{69}Br, as shown in Table IV, were obtained using Coulomb displacement energy calculations from Brown *et al.* [5] with our mass values for the mirror nuclei ^{65,66}Ge, ^{67}As, and ^{69}Se. The uncertainty of the Coulomb displacement is estimated to be 100 keV, which makes the present experimental mass measurement uncertainties negligible.

C. Neutron-proton pairing energy: V_{np}

Neutron-proton (np) pairing effects are expected to be maximized in $N = Z$ nuclei, due to the fact that the valence neutrons and protons occupy the same shell model orbits. Interest in np pairing has grown in recent years as radioactive ion facilities have been able to reach ever heavier $N = Z$ nuclei. An open question is how the np pairing energy behaves beyond $Z = 28$. It has been suggested by Jänecke [40] that the pairing energy should be a function of $\sqrt{A}$, while Van Isacker [9] suggested that the pairing energy arises from SU(4) symmetry which should be broken by large angular momenta and Coulomb interactions in heavier sd-shell nuclei, but could possibly be restored in nuclei beyond ^{56}Ni by a pseudo-SU(4) symmetry in the *pf*-shell.

TABLE V. Neutron-proton pairing energies for ^{66}As and ^{70}Br. In the first column, values are calculated using mass values from AME'03. In the second column, values presented in this work when available, otherwise using AME'03. In the third column, values are calculated as in column two except the mass of ^{70}Br used is from Davids *et al.* [36]. All values are in keV.

	AME'03	This work + AME'03	This work + AME'03 + Davids
^{66}As	−2460(750)	−3080(100)	–
^{70}Br	−2860(450)	−2960(330)	−3610(210)

The np pairing energy, V_{np}, for $N = Z$ nuclei can be extracted from nuclear binding energies, B, of a set of neighboring nuclei using the empirical formula [9]

$$V_{np} = [B_{N,Z} - B_{N-1,Z}] - [B_{N,Z-1} - B_{N-1,Z-1}]. \quad (3)$$

For $N = Z$ nuclei beyond ^{74}Rb, the mass values required for calculating V_{np} have not been measured. For ^{66}As and ^{70}Br the necessary mass values have had very large uncertainties or were only estimates. The new mass measurements can be used to reduce the uncertainty in V_{np} for both of these nuclei.

Table V lists the calculated np pairing energy based on mass values presented in this work compared with those calculated from literature values. The masses of $Z = N + 1$ nuclei required for Eq. (3) were calculated using Coulomb displacement energies and measured mirror nuclei masses. V_{np}(^{70}Br) was calculated using the Audi-Wapstra extrapolated mass value of ^{70}Br [31] in the first two columns of Table V. We find the Wigner energy for ^{66}As to be shifted by −620 keV, but still within the large uncertainty of the prior value while the value of V_{pn}(^{70}Br) is shifted by −100(550) keV.

A measurement of the β-decay Q-value of ^{70}Br reported by Davids *et al.* [36] has long been excluded from the Atomic Mass Evaluation based on disagreement with the expected two-neutron separation energies. As no other data on the mass of ^{70}Br has been published, we include the result from [36] for completeness and find V_{np}(^{70}Br) would be shifted by −750(490) in this case.

Figure 5 shows the neutron pairing energy for odd-odd $N = Z$ nuclei up to ^{74}Rb. As this figure demonstrates, based on our new data, there is an indication of a trend toward the restrengthening of V_{np}. Mass measurements of heavier $N = Z$ nuclei are required to clarify this trend.

D. rp-process

The even-even $N = Z$ nuclei ^{64}Ge,^{68}Se, and ^{72}Kr could be important waiting point nuclei in the astrophysical rp-process. The reasons are their relatively long half-lives as compared to the rp-process timescale of 10–100 s and the reduced proton binding energies of the odd-Z nuclei ^{65}As, ^{69}Br, and ^{73}Rb. However, depending on the actual proton capture Q-values, the delay caused by these waiting points can be decreased below their β-decay lifetimes by sequential $2p$ capture [1,6].

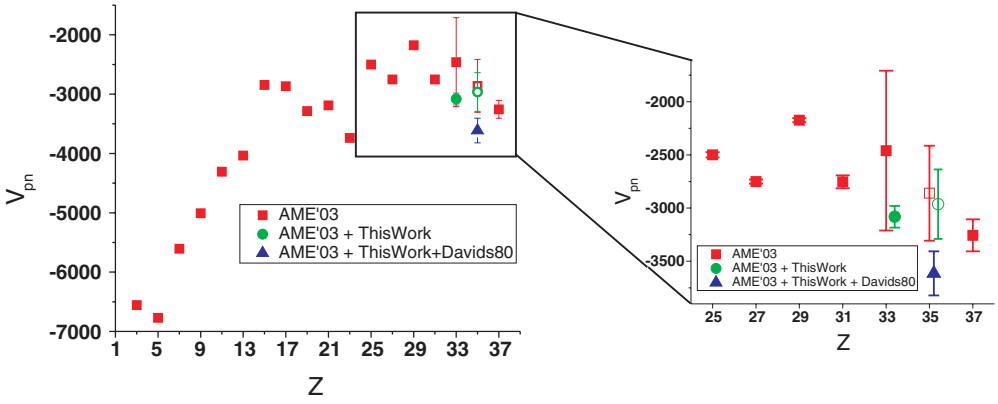

FIG. 5. (Color online) Neutron-proton paring energies as function of Z for odd-odd $N = Z$ nuclei up to ^{74}Rb. Open points incorporate AME'03 systematics. Closed points use only experimental data and Coulomb displacement energy calculations. Davids80 refers to [36].

Using the present mass measurements, along with the mass estimates from the Coulomb displacement energy, we can reduce the proton capture Q-value uncertainties for some of the nuclei which determine the effective lifetimes of the waiting point nuclei ^{64}Ge and ^{68}Se. For ^{64}Ge, our data yield a proton capture Q value, $Q_p = M(^{64}Ge) + M(p) - M(^{65}As)$, of $-255(104)$ keV. Similarly, we find ^{69}Br to be 216(150) keV more unbound than the value used in [14], further weakening proton capture on ^{68}Se. Table VI provides a comparison of the Q-values from the present mass measurements with previous values.

The reaction networks shown in Fig. 6 were used to determine the effective lifetimes of the waiting point nuclei ^{64}Ge and ^{68}Se. Network calculations were performed with a starting abundance of only the waiting point nuclide and protons, with the protons accounting for 70.5% of the mass fraction, corresponding to the solar value. Furthermore a density of 10^6 g/cm^3 was held constant in the calculations. Forward—(p, γ)—reaction rates were taken from [41], while reverse—(γ, p)—reaction rates were determined through detailed balance using the new Q-values presented. The change in the calculated forward rates due to the new Q-values were neglected as such changes are small compared to typical uncertainties in the Hauser-Feshbach reaction rate calculations. The temperature range used in these calculations was chosen because proton capture is ineffective for the high-Z nuclei considered here at temperatures below about 1 GK, while proton and photodisintegration inhibits proton capture at temperatures above 1.8 GK [6].

The results of these calculations are shown in Fig. 7. The open envelope represents the temperature dependance of the effective lifetimes based on one-sigma independent variations of all masses involved in the network using AME'03 values and CPT [14,15] data for ^{64}Ge and ^{68}Se. The filled area similarly depicts lifetimes using AME'03 and LEBIT data. Clearly, the LEBIT results considerably reduce the uncertainty in the effective lifetime of the two major waiting points, ^{64}Ge and ^{68}Se, in the rp-process. For ^{64}Ge the LEBIT results suggest that the waiting point can be bridged for a wider temperature range than previously believed. On the other hand, ^{68}Se causes a greater delay than previous data would have suggested. The significant shift in the temperature dependance of the lifetime of ^{68}Se is due to a 134 keV discrepancy found in the mass of ^{69}Se, resulting in the correspondingly large shift in $Q_p(^{69}Br)$ as shown in Table VI. These calculations also depend on the proton capture rates of ^{65}As and ^{69}Br, currently based on Hauser-Feshbach calculations [41] which can be very uncertain near the proton drip-line.

TABLE VI. Reaction Q-values derived from mass measurements and Coulomb displacement energies reported herein and derived from AME'03 [31]. All values in keV.

Reaction	This work	AME'03
^{64}Ge(p,γ)^{65}As	−255(104)	−354(172)[a]
^{65}As(p,γ)^{66}Se	2350(200)	2433(246)
^{68}Se(p,γ)^{69}Br	−679(119)[b]	−463(129)[b]
^{69}Br(p,γ)^{70}Kr	2450(216)	2234(227)

[a]Mass of ^{64}Ge from [15].
[b]Mass of ^{68}Se from [14].

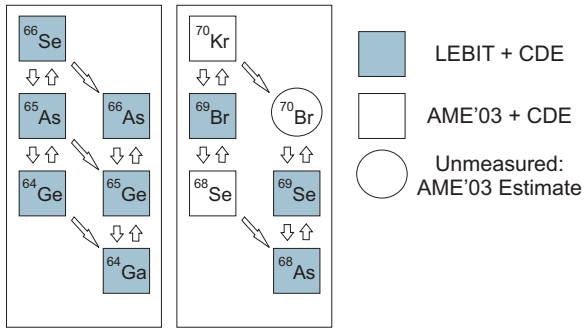

FIG. 6. (Color online) Networks used for the calculations of effective lifetimes for ^{64}Ge (left) and ^{68}Se (right). We also indicate the source of the mass excess values used in the calculation. CDE refers to Coulomb displacement energy.

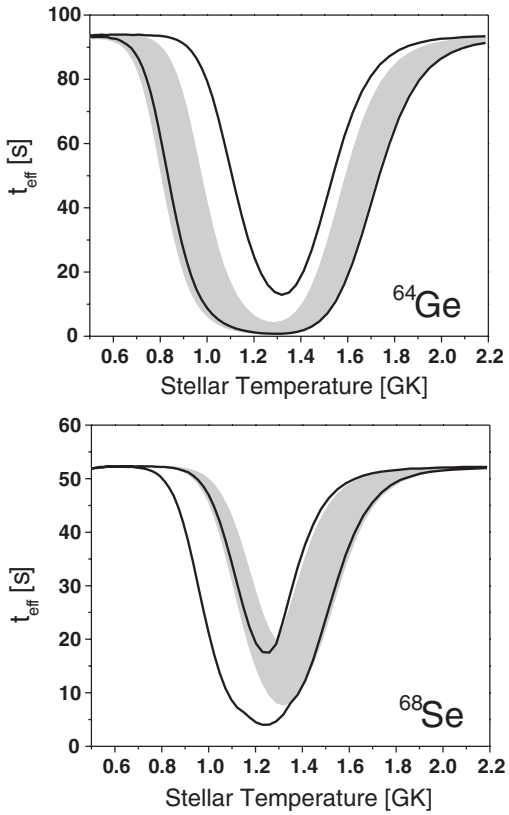

FIG. 7. Envelope of calculations of the effective lifetimes for ^{64}Ge (top) and ^{68}Se (bottom) for 1-σ variations of the atomic masses. The filled area results from LEBIT data, while the open envelope results from previous literature mass values.

VI. SUMMARY AND OUTLOOK

High-precision mass measurements of ^{64,65,66}Ge, ^{66,67,68}As, and ^{69}Se have been performed by means of Penning trap mass spectrometry. The rare isotopes were produced by heavy ion fragmentation with in-flight separation and thermalized with a gas stopping technique. ^{66}As, with a half-life of 96 ms, is one of the shortest-lived isotopes studied with a Penning trap. The mass measurement of ^{66}As, with an uncertainty of $\delta m/m = 4.1 \times 10^{-7}$, represents a 30-fold improvement in precision over previous measurements. In the case of ^{69}Se, the mirror of the unbound nucleus ^{69}Br, a 4σ deviation from earlier measurements has been found.

In combination with these mass measurements, calculated Coulomb displacement energies were used to estimate the masses of the mirror nuclei of several of the measured nuclei, leading to a considerable reduction in mass uncertainties in this region. The reduction in these uncertainties has lead to improvements of neutron-proton pairing energies for ^{66}As and ^{70}Br. The results support a trend toward increased np pairing strength with heavier $N = Z$ nuclei.

Astrophysical network calculations were performed with improved mass values. They indicate an enhanced waiting point nature for ^{68}Se and a decrease in the waiting point nature of ^{64}Ge. The new mass values are therefore likely to impact some existing X-ray burst models and should be used in future X-ray burst studies.

The factor dominating the uncertainty in the effective lifetime of ^{64}Ge are the masses of ^{65}As and ^{66}Se, which have been calculated via Coulomb shift energies. The uncertainty in the effective lifetime of ^{68}Se is dominated by uncertainty in the mass of ^{70}Kr, which has been calculated via Coulomb shift energy from ^{70}Se. The mass of ^{70}Se listed in 2003 Atomic Mass Evaluation is the weighted average of four independent mass measurements [42–45] which do not agree.

Mass measurements of heavier $N = Z$ nuclei at LEBIT are planned. Such measurements will hopefully provide further insight into neutron-proton pairing energies. Penning trap mass measurements of ^{68,70}Se have only very recently been performed at the LEBIT facility. These measurements will further reduce uncertainties in the effective lifetime of ^{68}Se. Based on our experience with ^{66}As, it may be possible to measure the mass of ^{65}As at the LEBIT facility and replace the predicted mass presented in this work with a precise experimental value. Planned improvements should also allow for a remeasurement of the mass of ^{66}As to a precision of $\delta m/m \leqslant 1 \times 10^{-8}$, which would make it a candidate for testing the conserved vector current hypothesis [46].

ACKNOWLEDGMENTS

We wish to acknowledge the support of Michigan State University, the National Science Foundation Grant PHY-0110253 and the U.S. Department of Energy Contract DE-FG02-00ER41144. H.S. acknowledges support from NSF grant PHY 0216783 (Joint Institute for Nuclear Astrophysics).

[1] H. Schatz, A. Aprahamian, J. Görres *et al.*, Phys. Rep. **294**, 167 (1998).
[2] R. Wallace and S. Woosley, Astrophys. J. Suppl. Ser. **45**, 389 (1981).
[3] O. Koike, M. Hashimoto, K. Arai *et al.*, Astron. Astrophys. **342**, 464 (1999).
[4] H. Schatz, A. Aprahamian, V. Barnard *et al.*, Phys. Rev. Lett. **86**, 3471 (2001).
[5] B. A. Brown, R. R. C. Clement, H. Schatz, A. Volya, and W. A. Richter, Phys. Rev. C **65**, 045802 (2002).
[6] H. Schatz, Int. J. Mass Spectrom. **251**, 293 (2006).
[7] E. Wigner, Phys. Rev. **51**, 106 (1937).
[8] P. Vogel, Nucl. Phys. **A662**, 148 (1999).
[9] P. Van Isacker, D. Warner, and D. S. Brenner, Phys. Rev. Lett. **74**, 4607 (1995).
[10] M. Chartier, G. Auger, W. Mittig *et al.*, Phys. Rev. Lett. **77**, 2400 (1996).
[11] G. F. Lima, A. Lépine-Szily, G. Audi *et al.*, Phys. Rev. C **65**, 044618 (2002).
[12] C. Guénaut, G. Audi, D. Beck *et al.*, Phys. Rev. C (accepted for publication).
[13] T. Eronen, V. Elomaa, U. Hager *et al.*, Phys. Lett. **B636**, 191 (2006).

[14] J. A. Clark, G. Savard, K. S. Sharma *et al*., Phys. Rev. Lett. **92**, 192501 (2004).
[15] J. A. Clark, Ph.D. thesis, University of Mannitoba, 2005.
[16] D. Morrissey, B. Sherrill, M. Steiner *et al*., Nucl. Instrum. Methods B **204**, 90 (2003).
[17] R. Ringle, T. Sun, G. Bollen *et al*., Phys. Rev. C (accepted for publication).
[18] G. Bollen, D. Davies, M. Facina *et al*., Phys. Rev. Lett. **96**, 152501 (2006).
[19] L. Weissman, P. Lofy, D. Davies *et al*., Nucl. Phys. **A746**, 655c (2004).
[20] L. Weissman, D. Morrissey, G. Bollen *et al*., Nucl. Instrum. Methods B **540**, 245 (2005).
[21] S. Schwarz, G. Bollen, D. Lawton *et al*., Nucl. Instrum. Methods B **540**, 474 (2003).
[22] R. Ringle, G. Bollen, D. Lawton *et al*., Eur. Phys. J. A **25**, supp.1, 59 (2004).
[23] H. Weick, H. Geissel, C. Scheidenberger *et al*., Nucl. Instrum. Methods B **164–165**, 168 (2000).
[24] R. Ringle, P. Schury, T. Sun *et al*., Int. J. Mass Spectrom. **251**, 300 (2006).
[25] R. Ringle, G. Bollen, A. Prinke *et al*., Int. J. Mass Spectrom. (in press).
[26] G. Bollen, R. B. Moore, G. Savard *et al*., J. Appl. Phys. **68**, 4355 (1990).
[27] N. Daly, Rev. Sci. Instrum. **31**, 264 (1960).
[28] F. Muntean and P. Armentrout, J. Chem. Phys. **115**, 1213 (2001).
[29] G. Bollen, *The Euroschool lectures on physics with exotic beams*, Vol. I (Springer, Berlin, 2004), p. 169.
[30] M. König, G. Bollen, H.-J. Kluge *et al*., Int. J. Mass Spectrom. Ion. Procress **142**, 95 (1995).
[31] A. Wapstra, G. Audi, and C. Thibault, Nucl. Phys. **A729**, 129 (2003).
[32] G. Bollen, H.-J. Kluge, M. König *et al*., Phys. Rev. C **46**, R2140 (1992).
[33] S. Becker, G. Bollen, F. Kern *et al*., Int. J. Mass Spectrom. **99**, 53 (1990).
[34] R. Birge, Phys. Rev. **40**, 207 (1932).
[35] J. A. Clark, K. S. Sharma, G. Savard *et al*., Phys. Rev. C (accepted for publication).
[36] C. Davids, Proceedings of the 6th International Conference on Atomic Masses and Fundamental Constants (AMCO-6), 1980, p. 419.
[37] G. Bollen, S. Becker, H.-J. Kluge *et al*., Nucl. Instrum. Methods A **368**, 675 (1996).
[38] J. C. Hardy, J. A. MacDonald, H. Schmeing *et al*., Phys. Lett. **B63**, 27 (1976).
[39] J. A. Macdonald, J. C. Hardy, H. Schmeing *et al*., Nucl. Phys. **A288**, 1 (1977).
[40] J. Jänecke, T. O'Donnell, and V. Goldanskii, Nucl. Phys. **A728**, 23 (2003).
[41] T. Rauscher and F.-K. Thielemann, At. Data Nucl. Data Tables **75**, 1 (2000).
[42] M. Chartier, W. Mittig, N. A. Orr *et al*., Nucl. Phys. **A637**, 3 (1998).
[43] M. Hausmann, J. Stadlmann, F. Attallah *et al*., Hyperfine Interact. **132**, 289 (2001).
[44] B. E. Tomlin, C. J. Barton, N. V. Zamfir *et al*., Phys. Rev. C **63**, 34314 (2001).
[45] G. F. Lima, A. Lépine-Szily, G. Audi *et al*., Phys. Rev. C **65**, 44618 (2002).
[46] J. Hardy and I. Towner, Phys. Rev. C **71**, 055501 (2005).